

Two-Fluid and Resistive Nonlinear Simulations of Tokamak Equilibrium, Stability, and Reconnection

S. Jardin 1), C. Sovinec 2), J. Breslau 1), N. Ferraro 1), S. Hudson 1), J. King 2), S. Kruger 4)
J. Ramos 3), D. Schnack 2)

1) Princeton University Plasma Physics Laboratory

2) University of Wisconsin

3) Plasma Science and Fusion Center, Massachusetts Institute of Technology

4) Tech-X Corporation, Boulder CO

e-mail contact of main author: jardin@pppl.gov

Abstract. The NIMROD and M3D / M3D- C^l codes now each have both a resistive MHD and a two-fluid (2F) capability including gyroviscosity and Hall terms. We describe: (1) a nonlinear 3D verification test in the resistive MHD regime in which the two codes are in detailed agreement, (2) new studies that illuminate the effect of two-fluid physics on spontaneous rotation in tokamaks, (3) studies of nonlinear reconnection in regimes of relevance to fusion plasmas with peak nonlinear reconnection rates that are essentially independent of the resistivity, and (4) linear two-fluid tearing mode calculations including electron mass that agree with analytic studies over a wide range of parameter regimes.

1. Introduction

The SciDAC¹ Center for Extended Magnetohydrodynamic Modeling (CEMM²) develops advanced computational models for the macroscopic dynamics of fusion-grade plasmas and implements these on some of the world's most powerful computers. The center is built around the 3D nonlinear simulation codes NIMROD[1] and M3D[2]. A new variant of M3D, called M3D- C^l [3], uses a split-implicit time advance applied to high order finite elements with C^l continuity. Here we describe recent verification and convergence tests related to resistive and two-fluid equilibrium, reconnection, and stability.

2. Sawtooth phenomena in a small ohmic tokamak

Both NIMROD and M3D have calculated the nonlinear evolution through three complete sawtooth cycles using the parameters of the CDX-U tokamak in the resistive MHD regime and find excellent agreement between the two codes in most all details of the simulation [4,5].

CDX-U is a small ($R_0=33.5$ cm), low-aspect-ratio ($R_0/a=1.5$) tokamak experiment with a typical operating temperature of about $T_e=100$ eV. Modelling 3D macroscopic activity in the experiment requires information on profiles, sources, and transport coefficients. The equilibrium profiles and inferred sources are provided by running the 2D free boundary flux-surface averaged transport timescale code TSC [6] to match typical traces of the plasma current $I_p(t)$ from the experiment. A sequence of experimentally relevant profiles, each at a fixed time, are obtained from the TSC computation as described in [5]. As the plasma current increases and the central current density also increases in the TSC calculation, the central safety factor q_0 , a measure of the pitch of the local magnetic field, falls monotonically in time. For the initial equilibrium used in the benchmark, we began from a TSC equilibrium where the central safety factor had fallen to $q_0=0.82$ and transferred this to be

¹ U.S.Department of Energy Scientific Discovery through Advanced Computing: www.scidac.gov

² w3.pppl.gov/CEMM

used as the initial state for the 3D calculations. The codes used a non-evolving Spitzer resistivity profile of the form $\eta \propto T_{eq}^{-3/2}$, normalized so that the central Lundquist number $S=1.94 \times 10^4$. The viscosity was held constant and uniform with a central Prandtl number $P_N \equiv \mu/\eta$ of 10. A high, uniform, and constant value of κ_{\perp} was chosen, equivalent to a physical value of approximately $200 \text{ m}^2/\text{s}$. The two codes differ in their implementation of parallel heat diffusion, with M3D using an “artificial sound wave” method in which a hyperbolic rather than parabolic operator convects heat along the field while NIMROD evaluates the actual anisotropic diffusion term. The parallel heat conduction parameter could therefore only be approximately similar in the two runs; it was chosen to correspond to an electron thermal speed six times the Alfvén speed. Source terms were added in the field and energy equations to drive these respective profiles toward their initial values.

The results obtained are shown for comparison in FIG. 1. After the first sawtooth cycle, the code results become relatively independent of the initial conditions. For each crash, the $n=1$ component first becomes linearly unstable and drives the other toroidal modes with $n>1$ through nonlinear coupling. We find that substantial $m>1$ islands are formed during the crash, but these quickly re-heal during the ramp phase. Even though many surfaces breakup during the crash phase, the temperature does not completely flatten due to the presence of residual surfaces and cantori which form effective heat barriers [7].

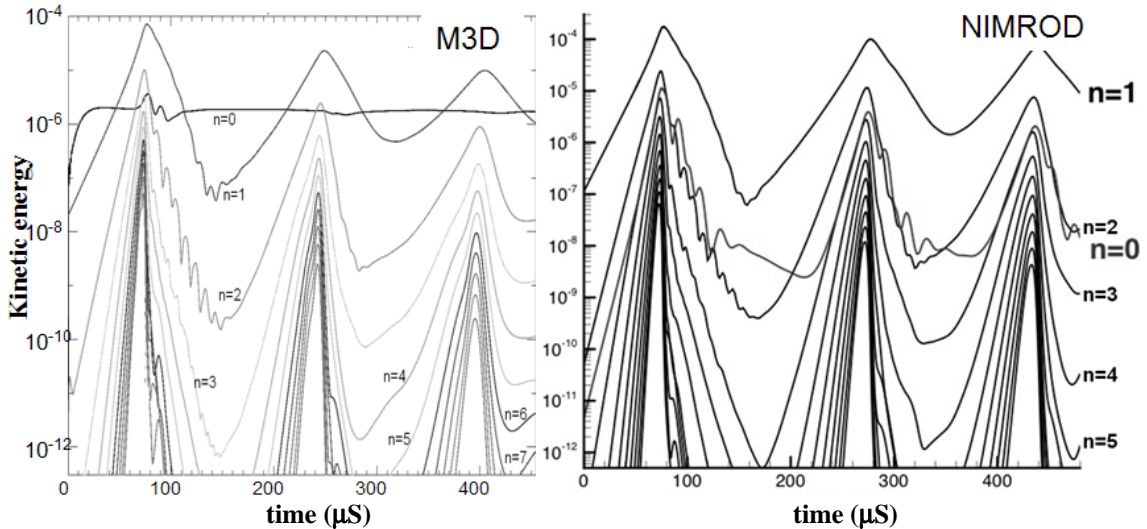


FIG 1: Time history of normalized kinetic energy by toroidal mode number during the first three sawtooth crashes in this iteration of the nonlinear CDX-U benchmark.

In order to define this problem in a way that is accessible to other 3D simulation codes, we propose that in the future, the codes be initialized with a semi-analytic definition of a stationary equilibrium configuration that closely approximates the experimental conditions. This can be done by specifying the pressures and densities as quadratic functions of the poloidal flux ψ , and giving a parametric form for the plasma boundary. Using the neo-classical resistivity and specifying a loop voltage V_{loop} , JSOLVER [8] can be used to calculate a unique resistive stationary equilibrium that satisfies: $V_{loop} = 2\pi\eta \langle \mathbf{J} \cdot \mathbf{B} \rangle / \langle \mathbf{B} \cdot \nabla \phi \rangle$, where the brackets denote flux surface average. The perpendicular heat conduction profile is initialized self-consistently to provide steady state profiles: $\kappa_{\perp} = V_{loop} \langle |\nabla \psi|^2 / R^2 \rangle / 2\pi\mu_0 T' \langle |\nabla \psi|^2 \rangle$, where the prime denotes the derivative with respect to the poloidal flux function ψ . After the first sawtooth cycle, the code results

should again become relatively independent of the initial conditions although the loop voltage remains as a boundary condition and the behaviour is expected to depend on the initial pressure profile through the function κ_L .

3. 2F NSTX equilibrium including flows

We have obtained axisymmetric steady-states of a comprehensive, dissipative two-fluid model applied to NSTX³ geometry plasmas by integrating the nonlinear dynamical equations

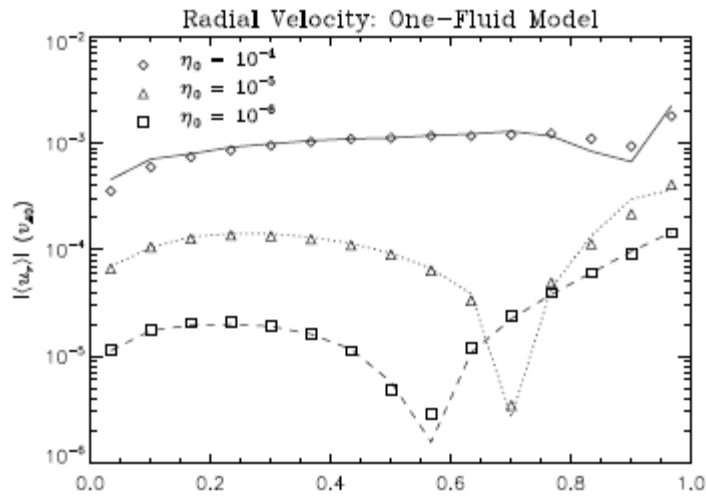


FIG 2: The Surface-averaged radial velocity from simulation results (points) compared to Pfirsch-Schlüter theory (lines) for a range of resistivities.

realistic inductive current drive, Ohmic heating, and particle injection models, and may therefore reach a realistic steady-state in the presence of dissipation. Third, the model used here includes both parallel viscosity and gyroviscosity [13], which have important

using M3D-C¹ [9]. These solutions go beyond previous calculations in several ways. First, dissipative effects such as viscosity and resistivity are included, which are not present in most other numerical methods for obtaining such steady-states [10-12]. Our results also go beyond those obtained using other methods which do include dissipative effects, because the implicit time-step method in M3D-C¹ allow us to carry the time-integration sufficiently far so that the results are stationary on all physical time-scales present in the problem.

Second, these simulations include

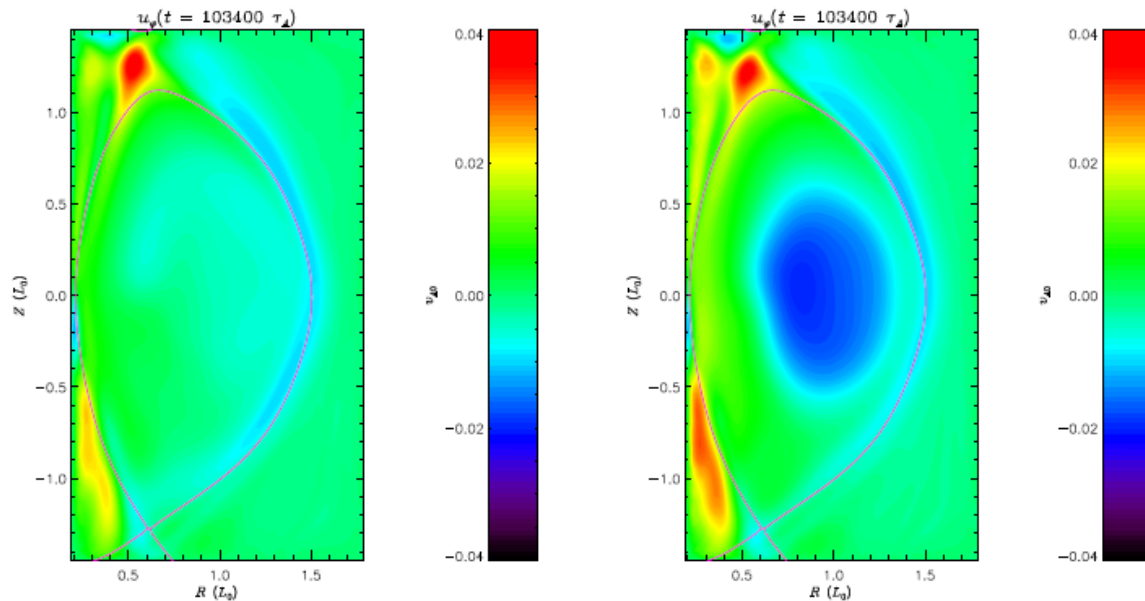


FIG 3: The steady-state toroidal velocity in two simulations with density injection on the low-field side. On the left, gyroviscosity has been omitted; on the right, it is included.

³ National Spherical Torus Experiment (PPPL)

implications for the steady-state flows, and which have not been included in any other studies of this type. Finally, two-fluid effects are also included, which are not present in any comparable published work.

In these solutions, a number of interesting results have been found, some of which have not previously been observed or predicted. The surface-average of the radial flows have been found to be in excellent agreement with Pfirsch-Schlüter theory (see FIG 2). It is also found that strong, up-down asymmetric edge flows may exist in highly resistive scrape-off layers, in accordance with previous simulation results [14].

Gyroviscosity is found to play an important role in the steady-state flows; driving toroidal flows in the presence of a density source (see FIG 3). The magnitude and direction of the toroidal gyroviscous force is dependent on the position of the density injection. The inclusion of gyroviscosity is found also to result in strong, regular oscillations in highly resistive steady-states. Parallel viscosity has been demonstrated to damp poloidal flows significantly, as previously anticipated [15].

Future work will focus on moving to more realistic parameter regimes. Modifications to the electron parallel viscosity which allow the inclusion of some important collisionless neoclassical effects, such as the bootstrap current, will be explored. More sophisticated transport models, which should allow the simulation of H-mode plasmas, will also be incorporated. Furthermore, we plan to use M3D- C^I to explore the three-dimensional linear stability of the axisymmetric equilibria that we have obtained. This work should facilitate an understanding of the effect of flows, finite Larmor orbits, and other non-ideal effects on the linear growth of ELMs and other instabilities.

4. Nonlinear 2F reconnection with an arbitrary guide field:

We have benchmarked NIMROD and M3D- C^I by performing convergence studies on the GEM two-fluid nonlinear reconnection problem. Results for the M3D- C^I code applied to the zero guide field original GEM challenge case [16] are shown in FIG 4 and FIG 5.

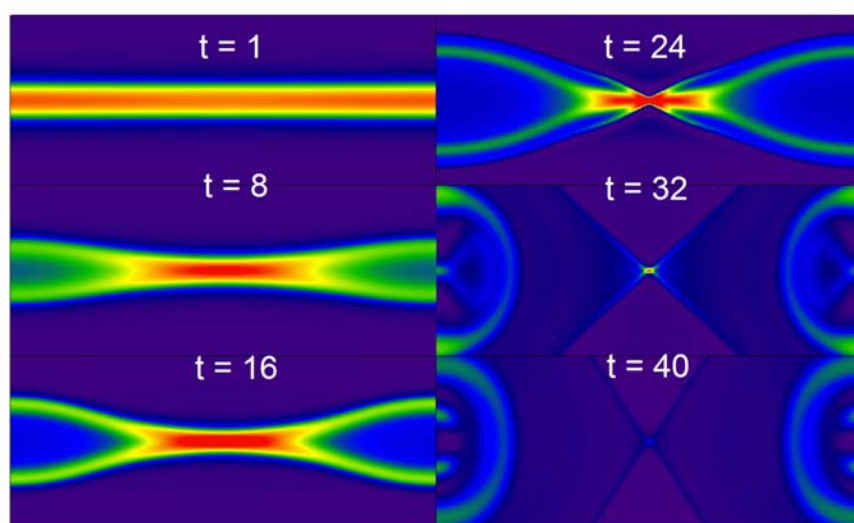


FIG 4: Contours of the toroidal current density at selected times. Note that a transition occurs between the time of $t=16$ and $t=32$.

In this study we used the geometry and units of Ref. [16] with normalized resistivity $\eta=0.005$, viscosity $\mu=0.05$, and thermal conductivity $\kappa=0.02$. The time-step Δt varied from 0.05 to 0.20 to satisfy convergence criteria, with an average value of 0.10. A triangular mesh with uniform node spacing of h was used with the number of nodes varying from 120^2 to

210^2 as indicated. A hyper-resistivity was included of strength $\lambda = C_H h^2$ with $C_H = d_i = 1.0$ as discussed in [3] to regularize the solution.

We have extended the problem of nonlinear magnetic reconnection in a Harris current sheet to include a strong guide field to better approximate nonlinear reconnection in tokamaks and to obtain scaling relations and project resolution requirements to the ITER regime. Our interest is in the regime: $\delta \ll \rho_s \ll d_i$, $\beta \ll 1 \sim \beta_p$. Here, δ is the Sweet-Parker reconnection thickness, $\rho_s = \sqrt{\beta d_i}$ is the ion sound gyro-radius, and $d_i = c/\omega_{pi}$ is the ion skin depth. In the absence of electron inertia, all calculations

required an effective hyper-resistivity λ_H proportional to d_i in order to resolve the singularity at the x-point. The reconnection rate decreases with increasing λ_H , but asymptotes to a value independent of λ_H .

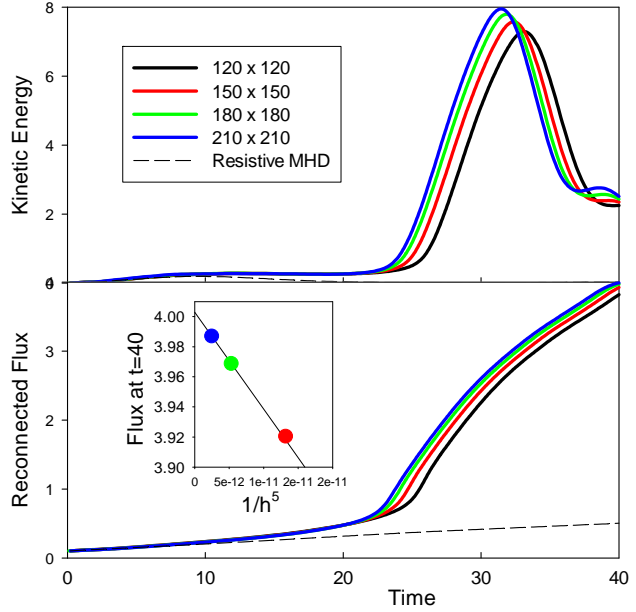


FIG 5: Convergence study in grid size with M3D-C1 code for zero guide field two-fluid GEM reconnection. Inset shows convergence as $\sim h^5$ as expected.

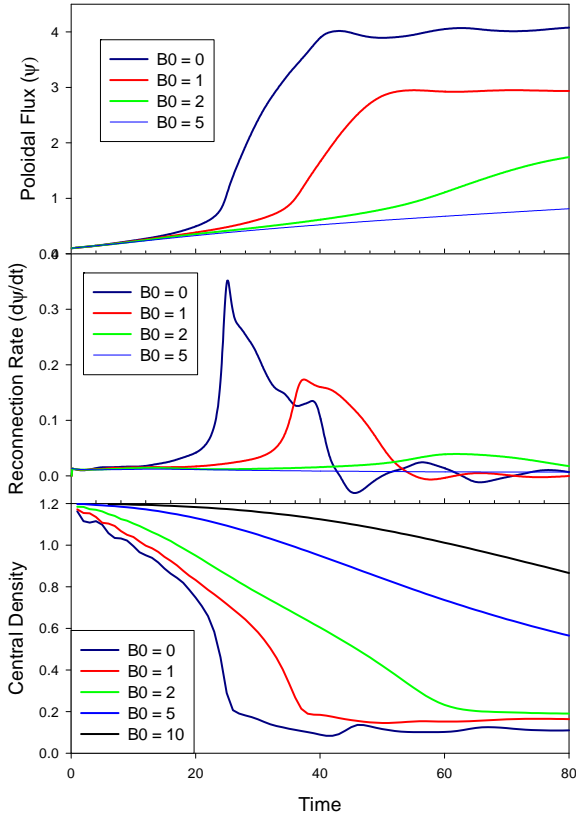


FIG 6: Guide field added to GEM reconnection problem dramatically reduces reconnection rate.

It can be seen from FIG 6 that the reconnection rate decreases markedly with increasing guide field. This is partly due to the evolution of the density and the effect of the guide field in reducing compressibility. As seen in the bottom frame of FIG 6, the density depletes in the reconnection region for the zero or small guide field case, thus increasing the effective d_i . This density reduction does not occur nearly as much when the guide field is increased. If density evolution is not included in the simulation, we find that for fixed d_i , the guide field still reduces the rate of magnetic reconnection but not as dramatically. We further find that increasing $\beta \equiv \frac{5}{3} p_0 / B_0^2$ increases the reconnection rate.

We have performed a series of calculations varying parameters in the range: guide field: $0 \leq B_0 \leq 5$; ion skin depth: $1 \leq d_i \leq 8$;

central pressure: $0.25 \leq p_0 \leq 1.0$; viscosity:

$0.005 \leq \nu \leq 0.05$; resistivity: $0.0005 \leq \eta \leq 0.005$. The density was held constant in these calculations since the initial conditions (of peaked density) were such as to make the density depletion the dominant effect when its evolution was included. We performed a least squares fit of the maximum reconnection rate for these constant density calculations to the formula:

$$\psi_{MAX} \sim \left[\frac{\beta}{1+\beta} \right]^A d_i^B \nu^C \eta^D$$

This gave the values $A=.95$, $B=.45$, $C=-.33$, $D=.05$. The weak dependence on resistivity implies that resistivity is not a factor in 2F nonlinear reconnection when a high guide field is present. These studies were done with a complete 8-field 2F model (without density evolution). In order to relate to some previous studies, we have repeated some of the calculations with the reduced 4-field model [17]. We find that the 4-field model does a fairly good job at reproducing the evolution at high guide field strengths, but not as good at low field strengths.

5. Two-fluid linear tearing in different parameter regimes:

Tearing instabilities represent a balance of destabilizing equilibrium gradients and restoring responses at large scales with reconnection physics at small scales. In two-fluid models, the reconnection scale interacts with larger scales through an intermediate response that is analogous to dispersive whistler-wave and kinetic-Alfvén-wave (KAW) dynamics. As summarized in Ref. [18], the response for a particular situation depends on the strength of the instability (measured by the tearing eigenvalue Δ') and on the size of the ‘sound gyroradius,’ $\rho_s = c_s/\Omega_i$, where c_s is the ion acoustic speed and Ω_i is the ion gyroradius, relative to the reconnection scale. Numerical two-fluid models intended for a wide variety of applications need to be able to reproduce the important transitions over quantitatively correct ranges in the parameter space. Analytical dispersion relations derived in slab geometry with hyperbolic-function equilibria are particularly convenient for verifying numerical computations, because there is a simple closed-form relation for computing Δ' . In the following, we compare results from the NIMROD code using its implicit leapfrog advance for the two-fluid model [19] with two analytical scalings over parameter space.

The computations described here have large guide-field (25-50 times larger than the reconnecting field) and satisfy the tearing condition of $\Delta'\delta \ll 1$, where δ is the generalized skin depth $\sqrt{d_e^2 + \eta/\mu_0\gamma}$, with d_e , η , and γ being the electron skin depth, electrical resistivity, and growth-rate, respectively. The first set of computations varies $\rho_s = \sqrt{\beta}d_i$ by varying β , the square of the ratio of ion acoustic and Alfvén speeds, while maintaining fixed ion skin depth d_i .

Numerical results shown in FIG. 7a extend from the MHD limit of $\rho_s \ll \delta$, through the KAW-response range, and into the large- ρ_s regime, where diffusion limits two-fluid effects [18]. Over the two-fluid regimes, quantitative values from computations converged with more than 100 biquartic finite elements over the direction of inhomogeneity and concentrated near the reconnection layer agree with analytical results evaluated from Ref. [18] to approximately 7%. The discrepancy is attributable to practical difficulties in satisfying all orderings assumed for the analytics. The computations need to include the reconnection

scale, which can be an order of magnitude smaller than δ , the sound gyroradius scale, the equilibrium scale (L), and a larger global scale to match analytical solutions where the domain is not bounded. Through numerical experimentation, we find that the computational boundaries need to be at least a factor of six beyond the equilibrium scale for growth rates to be independent of wall location. The parameters used for FIG. 7a have $\delta/L \cong 8\%$, which is marginal for achieving asymptotic reconnection but practical for the parameter scan with the computational domain extending three orders of magnitude beyond the reconnection scale. Better quantitative comparison with the asymptotic analysis is achieved as resistivity, hence δ/L , is reduced. The discrepancy in the resistive-MHD limit of FIG. 7a arises from the analytical derivation, which assumes a two-fluid response.

We have recently derived another form of the dispersion relation that assumes a minimal level of plasma pressure, $S^{-2/5} \ll \beta \leq 1$ where S is the Lundquist number, and is valid for both MHD and two-fluid responses [20]. The only small parameter in the derivation is $\varepsilon_\eta \equiv 1/S$. In these conditions, the dispersion relation is independent of the value of β , and the importance of two-fluid effects is controlled by d_i alone. FIG 7b compares the second set of numerical results with the dispersion relation for these conditions. The transition from resistive-MHD to two-fluid tearing is quantitatively verified, and we surmise that the quantitative agreement is facilitated by the fact that the analysis requires fewer orderings to be satisfied.

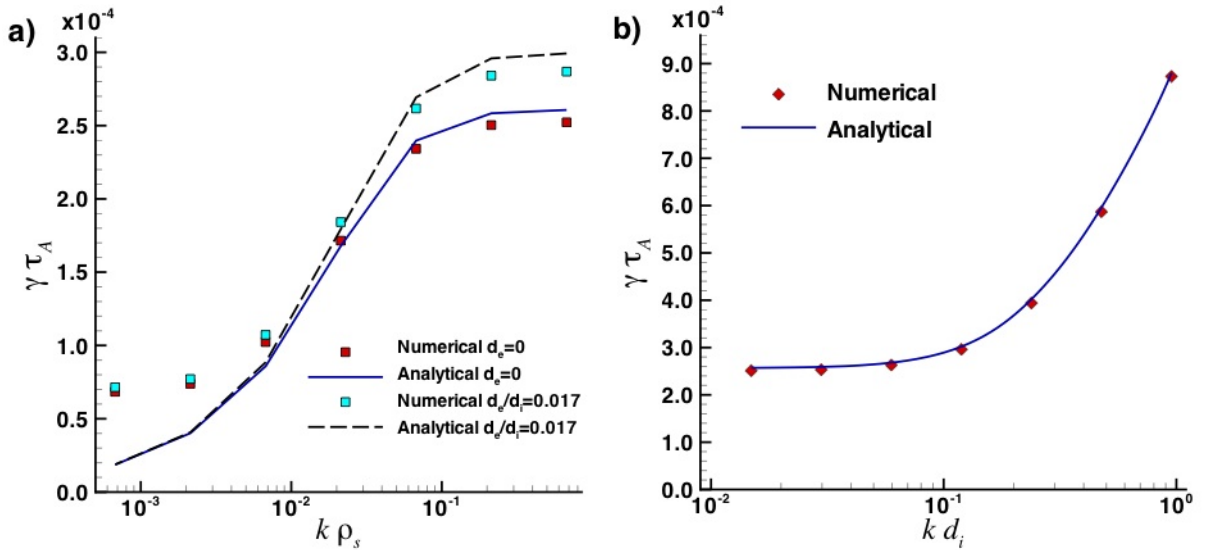


FIG. 7. Comparison of numerical tearing-mode growth rates at $S = 7.0 \times 10^5$ from the NIMROD code with a) asymptotic analysis in Ref. [18] for conditions with $\Delta'/k = 0.30$, $kL = 0.93$, and $k d_i = 2.3$ and b) the analysis in Ref. [20] for $\beta \gg S^{-2/5}$ and $d_e = 0$ with $\Delta'/k = 1.45$, $kL = 0.76$, and $\beta = 0.083$. Here, $\tau_A \equiv \sqrt{\mu_0 \rho} / k B_{y_\infty}$, where k is the wavenumber in the periodic direction, and B_{y_∞} is the magnitude of the reconnecting field; $S \equiv \mu_0 / \eta k^2 \tau_A$.

6. Acknowledgements

The authors would like to thank W. Park, G. Fu, J. Chen, H. Strauss, and L. Sugiyama for valuable discussions regarding and contributions to this study. Calculations were performed at the National Energy Research Scientific Computing Center (NERSC), which is supported by the Office of Science of the U.S. Department of Energy under Contract No. DE-AC02-

05CH11231, and at the National Center for Computational Sciences (NCCS). This work was supported by U.S. DoE contract DE-AC02-76CH03073, and Grant No. DE-FC02-02ER54668 and by the SciDAC Centre for Extended MHD Modelling (CEMM)

7. References

- [1] SOVINEC, C., et al., “Nonlinear magnetohydrodynamics simulation using high-order finite elements”, *J. Comput. Phys.*, **195** 355 (2004)
- [2] PARK W., et al., “Plasma simulation studies using multilevel physics models”, *Phys Plasmas* **6**, 1796 (1999)
- [3] JARDIN, S., et al., “A high-order implicit finite element method for integrating the two-fluid MHD equations in two dimensions”, *J. Comput. Phys.*, **226** 2146 (2007)
- [4] BRESLAU J., et al., “An Improved tokamak sawtooth benchmark for 3D nonlinear MHD”, *Comm. in Comput. Phys.* **4** 647 (2008)
- [5] BRESLAU J., et al., “Three-dimensional modeling of the sawtooth instability in a small tokamak”, *Phys. Plasmas* **14** 056105 (2007)
- [6] JARDIN, S., et al., “Dynamic modeling of transport and positional control of tokamaks”, *J. Comput. Phys.* **66** 481 (1986)
- [7] HUDSON S., et al., “Temperature contours and ghost surfaces for chaotic magnetic fields”, *Phys. Rev. Lett.*, **20** 203201 (2008)
- [8] DELUCIA J., et al., “An iterative metric method for solving the inverse tokamak equilibrium problem”, *J. Comput. Phys.*, **37** 183 (1980)
- [9] FERRARO N. “Non-ideal effects on the stability and transport of magnetized plasmas”, PhD Thesis, Princeton University, Dept. of Astrophysical Sciences (2008)
- [10] SEMENZATO, et al., “Computation of symmetric MHD flow equilibria”, *Comp. Phys. Rep.*, **1** 389 (1984)
- [11] BELIAEN A., et al, “FINESSE: Axisymmetric MHD equilibria with flow”. *J. Comp. Phys.*, **182** 91 (2002)
- [12] GUZZOTTO L., et al., “Magnetohydrodynamics equilibria with toroidal and poloidal flow” *Phys. Plasmas*, **12** 056107 (2005)
- [13] FERRARO, et al., “Finite element implementation of Braginskii's gyroviscous stress with application to the gravitational instability” *Phys. Plasmas* **13** 092101 (2006)
- [14] AYDEMIR A., “Shear flows at the tokamak edge and their interaction with edge-localized modes” *Phys. Plasmas* **14** (2007)
- [15] HASSAM, A., et al., “Time evolution of mass flows in a collisional tokamak” *Phys. Fluids*, **21** 2271 (1978)
- [16] BIRN J., et al., “Geospace Environmental Modeling (GEM) Magnetic Reconnection Challenge”, *J. Geophys. Res.*, [Space Phys.] **106** 3715 (2001)
- [17] FITZPATRICK, R. et al, “Collisionless magnetic reconnection with arbitrary guide field”, *Phys Plasmas* **11** (2004) 4713
- [18] MIRNOV V., et al., “Two-fluid tearing instability in force-free magnetic configuration”, *Phys. Plasmas* **11**, 4468 (2004).
- [19] SOVINEC C., et al, “Nonlinear extended magnetohydrodynamic simulation using high-order finite elements”, *J. Phys.: Conference Series* **16**, 25 (IoP, London, 2005)
- [20] AHEDO E., et al, “Parametric analysis of the two-fluid resistive tearing instability”, Massachusetts Institute of Technology report PSFC/JA-08-28 (September 2008); RAMOS J., “Progress in the two-fluid theory of the tearing mode”, Meeting of the Center for Extended MHD Modeling, Boulder C) (April 2008)
<http://w3.pppl.gov/cemm/Sherwood2008/Ramos.pdf>